This is an *Accepted Manuscript*, which has been through the Royal Society of Chemistry peer review process and has been accepted for publication.

Accepted Manuscripts are published online shortly after acceptance, before technical editing, formatting and proof reading. Using this free service, authors can make their results available to the community, in citable form, before we publish the edited article. We will replace this *Accepted Manuscript* with the edited and formatted *Advance Article* as soon as it is available.

You can find more information about *Accepted Manuscripts* in the **Information for Authors**.

Conductive polymer nanocomposites with hierarchical multi-scale-structure via self-assembling carbon-nanotubes on graphene on polymer-microspheres

Changyu Tang[a*], Gucheng Long[a,b], Xin Hu[a], Ka-wai Wong[a], Woon-ming Lau[a], Meikun Fan[a], Jun Mei[a], Tao Xu[c], Bin Wang[b*], David Hui[d]

a. Chengdu Green Energy and Green Manufacturing Technology R&D Center, CAEP Chengdu Development Center of Science and Technology

b. Chemical Synthesis and Pollution Control Key Laboratory of Sichuan Province of China, School of Chemistry and Chemical Industry, China West Normal University, Nanchong, China.

c. Institute of Chemical Materials, China Academy of Engineering Physics, China.

d. Department of Mechanical Engineering, University of New Orleans, New Orleans, USA

ABSTRACT

A novel and highly conductive 3-dimensional (3D) hierarchical multi-scale structure is formed with a new, simple, facile, and water-based method to enable practical production of conductive carbon nanofiller/polymer composites. More specifically, π-π interaction between CNTs and graphene oxide (GO) is exploited to disperse conductive but non-polar CNTs with amphiphilic GO sheets to form a stable aqueous colloidal solution. Aqueous-dispersible latex-polystyrene microspheres are then added to enable the self-assembling processes of anchoring CNTs on GO and wrapping microspheres with GO-stabilized CNTs for the formation of an intriguing 3D hierarchical multi-scale structure. Amid this process, GO is reduced to become conductive reduced-graphene-oxide (RGO). The resultant RGO sheets act as a "nano-wall" to prevent CNT from randomly diffusing into the polymer bulk during thermal pressing of RGO-CNT/microspheres, which results in the formation of a 3D foam-like network of RGO-CNT with high quality. The resultant composite with such

---
* Address correspondence to: sugarchangyu@163.com (C.Tang); wangbin6251@126.com (B. Wang).

structure gives an ultra-low percolation threshold (0.03 vol% RGO-CNT) and a reasonably high conductivity (153 S/m at 4 vol% RGO-CNT), which could satisfy various applications compromising transparency and electrical conduction characteristics (eg. transparent antistatic coatings, capacitive touch-screen, and transparent electronic devices).

KEYWORDS: graphene; carbon nanotube; 3D network; self-assembly; polymer composite

A table of contents entry
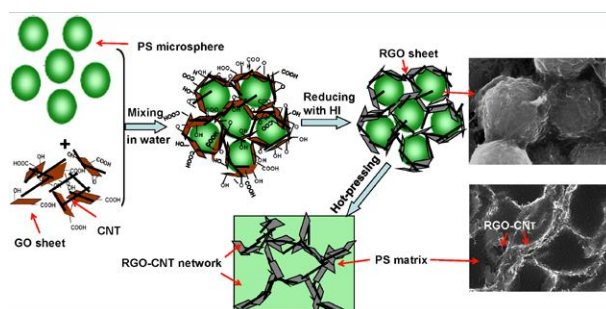
GO is employed to disperse CNTs and direct their assembly on Polystyrene microspheres to form 3D hierarchical conducting network.

1. **Introduction**

The development of well-designed 3-dimensional (3D) hierarchical structures from low-dimensional nano-scale building blocks fuels wide scientific and technological interests because such 3D hierarchical multi-scale structural designs are known to translate the excellent properties of nanomaterials into new macroscopic properties for practical applications[1-10]. Particularly, various 3D hierarchical structures consisting of 1D and 2D nanomaterials (as shown in Figure 1), which combine the original functions from two components but generate more unexpected properties exceeding the sum of the properties of the individual building blocks, are becoming more and more attractive for various applications[11-15]. For example, new emerging 2D single-atomic-thick graphene and 1D carbon nanotube (CNT) [16, 17], which both own large surface area and high electrical conductivity，were recently fabricated into 3D hierarchical hybridized structures, with versatile fascinating properties, including surface area, surface activity and electrical conductivity, for functional applications such as hydrogen storage agents, catalysts, electrochemical electrodes, and electrically conductive polymer composites [18-23].

In the emerging field of electrically conductive polymer composites (CPCs), those composites filled with carbon nanofillers (such as CNTs and graphene) have been used successfully for various electrical applications such as antistatic protection, electromagnetic shielding, electrode plates of fuel cells, and flexible electronics[24-27]. Typically, these CPCs are lightweight, inexpensive, flexible, oxidation-resistant, and easy to process. One of the current critical issues in the advancement of high-performance CPC applications is reducing filler percolation threshold and increasing conductivity. Here, achieving as low as possible filler percolation threshold can result in several important benefits such as reducing production cost, keeping the good processability of polymers, and minimizing the loss of optical transparency of the polymer matrix for electronic device application[25,28].

Generally, the conductivity and percolation threshold of CPCs strongly depend on filler type and conductive network structure[29, 30]. Therefore, design and construction of 3D hierarchical CNT-graphene network structures with excellent properties

3

promise a new strategy to satisfy the aforementioned requirements of excelling CPC properties. However, to the best of our knowledge, in-situ preparation of CPCs with such structures is rarely reported [22]. It could be due to the fact that most preparation methods for CPCs such as melting blending, solution blending and latex blending are currently limited by their ability to precisely constructing high quality 3D conducting network by CNT and graphene[25,31]. While researchers are still struggling with the process, in fact, various elaborate 3D hierarchical structures building up with tiny nanoscale blocks have widely existed in biological organisms (e.g. bone, teeth, and hair) and these super-architectures are generally precisely controlled by self-assembly process in aqueous environment, which is driven by some known interactions including hydrogen bonding, electrostatic adsorption, and van der Waals force[32-34].

Latex blending could be a very suitable method for imitating nature to accomplish self-assembly of carbon nanofillers with polymer to construct 3D structures with high quality[35, 36]because it includes the key elements for driving self-assembly such as aqueous environment and devisable surface functionalities on 3D polymer-latex microspheres. Ideally, polymer-latex microspheres can act as a template to direct carbon nanofillers around them to form ordered 3D segregated network structure. The polymer composites with this structure are proven to exhibit much better electrical properties than those with randomly dispersed filler structure[27,37]. However, successfully constructing 3D segregated network structure with high quality by latex blending still faces two big challenges. First, both conductive graphene and CNTs, which have no polar functionalities, are lack of driving forces for self-assembly on latex microsphere and tend to aggregate in the solution. The most widely adopted remedies are inserting polar chemical groups such as -COOH and –OH directly to graphene and CNTs or adding surfactants such as alkyl-sulfates to indirectly raise the polarity of CNTs[23,25,38, 39], but both remedies compromise the conductivity of the resultant graphene or CNT network. Another challenge is the difficulty in controlling the location and distribution of carbon nanofiller in the polymer matrix during latex microsphere coalescence to form the final composite. For example, it was often observed that one-dimensional CNTs easily transfer into polymer latex microspheres

from the CNT/latex-microsphere boundary when latex microspheres are coalesced and deformed during drying or hot-compaction at elevated temperature[37]. This behavior leads to the breakage of segregated CNT network and CNTs randomly disperse among polymer matrix with weak connection.

Here we report a simple, facile and water-based method to form 3D hierarchical structures with high quality by self-assembling conductive CNTs (nano-1D), conductive graphene sheets (nano-2D), and polystyrene-latex microspheres (micro-3D). The method takes advantage of the following scientific and technical considerations: (a) all three building blocks can be modified to become compatibly dispersed in water; (b) amphiphilic GO as graphene's precursor is employed to disperse and anchor pristine CNTs by π-π interaction[40]; (c) GO-stabilized CNTs effectively wrap each latex microsphere by self-assembly followed by in-situ chemical reduction and the resultant reduced graphene oxide (RGO) sheets act as "nano-wall" to prevent CNT from randomly diffusing into the polymer microsphere during CPC formation. Comprehensive measurements and analyses are performed to demonstrate the superior structural and functional properties of the resultant CPCs in reference to the data from CPCs prepared by conventional techniques.

Clay or graphene
CNT
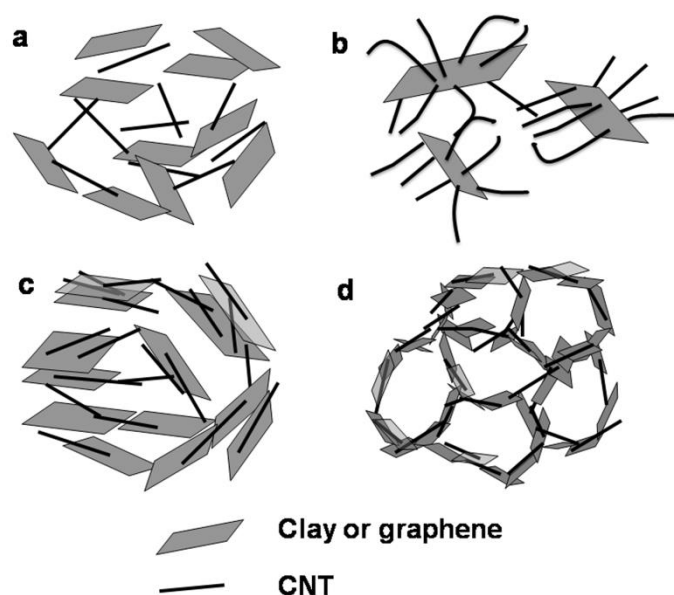
Figure 1. Various 3D hierarchical structures consisting of 1D and 2D nanomaterials. (a) Disordered and loose 3D hybrid, in which some of CNT and clay do not take part

in the formation of hybrid network due to insufficient interaction between them. Most joints between CNT and clay are point-to-point contacts [11]. (b) 3D hybrid from CNT grown on graphene (or clay) showing strong adhesion between CNT and graphene (or clay) [13]. (c) Compact and disordered 3D hybrid of graphene and CNT, in which these fillers interconnect in face-to-face contact way due to strong π-π interactions between them [15]. (d) Foam-like 3D hybrid of graphene and CNT (our work).

2. Experimental

2.1 Materials.

Natural graphite powders with an average particle size of ~20 μm were purchased from Qingdao Black Dragon Graphite Co., Ltd. Potassium permanganate, sulfuric acid (98%), hydrogen peroxide (>30%), sodium nitrate, hydrogen iodide (>45%), sodium dodecyl sulfate (SDS), alcohol (>99%) , and tetrahydrofuran (THF) were purchased from Changzheng Chemical Reagent Company (Chengdu, China). Multi-wall carbon nanotubes (MWNTs, purity > 95%, 10 nm in diameter, 2 μm in length) manufactured by CVD were purchased from Nanocyl S.A. (Belgium). GO was prepared from graphite as the starting material according to Hummer's methods[41]. Poly (vinyl pyrrolidone) (PVP, Mw=36000) and azobisisobutyronitrile (AIBN) were used as a stabilizer and initiator respectively for preparing PS latexes. Styrene monomers were purified to remove the inhibitors before polymerization.

2.2 Preparation of PS latex suspension

Mono-dispersed PS latexes were prepared in a three-necked flask by dispersion polymerization under nitrogen as described in previous literatures[36]. Typically, styrene monomers (20.0 g) and a radical initiator of AIBN (0.3 g) were dissolved in ethanol (60.0 g) containing PVP (2.0 g) as a stabilizer at room temperature. Nitrogen bubbling was applied for 20 minutes to remove oxygen in the mixture. The mixture was stirred at 200 rpm and at 70 $^{\circ}$C for 12 h. The obtained mono-dispersed PS microspheres were washed with ethanol and water respectively for several times to remove any unreacted styrene and PVP. Finally, the PS microspheres were dispersed into water to form a suspension for later use.

2.3 Preparation of Reduced GO-CNT /PS CPC (RGO-CNT /PS CPC)

In a typical procedure, a GO solution (0.5 mg/mL) was prepared by dispersing 10 mg GO powders into 20 mL water under sonication at 100 W for 15 min. 10 mg pristine CNTs were added into resultant GO solution with stirring for 1 h and sonication for 20 min to form a homogenous black suspension (1:1 weight ratio of CNT/GO). Subsequently, the white PS microsphere suspension was mixed with GO-CNT by mechanical stirring for 30 min. A black coagulation was observed in the suspension, indicating the self-assembly of PS microspheres with GO-CNT nano-filler in water. After that, the coagulation was isolated by filtration and was subjected to chemical reduction with 45 wt% HI solution at 90 ^{o}C for 2 h. The reduced coagulation was then washed with water three times and dried under vacuum. Finally, the resultant RGO-CNT/PS powder was hot-pressed at 1.0 MPa at 200 ^{o}C for 15 min, to form a disc film with a diameter of 25 mm and thickness of ~0.3 mm. For comparison, SDS was used to disperse CNTs to form a dispersion of a weight ratio of 1:1 and was mixed with PS microspheres for preparing SDS-CNT/PS composites by similar subsequent procedure as for RGO-CNT/PS composites.

The mass fraction of conductive fillers in polymer composite was converted to a volume fraction (φ) by the following equation:

$$\varphi = \frac{m_f \rho_p}{1 + m_p \rho_f}$$

where m_f and m_p are the mass fraction of conductive filler and polymer respectively, and ρ_f and ρ_p are the density of conductive filler and polymer. The density of CNT, GO (or RGO) and PS can be taken as 2.2, 2.2, and 1.05 g/cm^3, respectively.

2.4 Measurements and characterizations

Microscopic observation. Atomic force microscopy (AFM) images of GO sheets were taken from an SPA 400/SPI 4000 (Seiko Instruments) microscope in the tapping mode. The sample for AFM testing was prepared by spin-coating a GO solution on a freshly cleaved mica surface at 1000 rpm and dried at 60 ^{o}C in vacuum. The morphologies of PS microspheres, their composites and fillers were examined by

7

scanning electron microscopy (SEM, S5200, Hitachi Company) under an acceleration voltage of 3 kV. The TEM measurement was carried out with a Tecnai G2 F20 electron microscope (FEI Company) under a voltage of 100 kV.

Spectral analysis. UV-Vis absorption spectra of SDS-CNT and GO-CNT suspensions were measured with a UV-Vis spectrophotometer (SP-756, Shanghai Spectrum Co. Ltd., China) in the range of 200–800 nm to examine the dispersion of both CNT suspensions. FTIR spectra of GO, PS microsphere, and PVP were measured with a Nicolet 560 Spectrophotometer in the range of 4000-400 cm^{-1} under the transmittance mode. The samples were mixed with KBr powder, and the resulting mixtures were pressed into disks (about 0.3 mm in thickness) for FTIR test. X-ray photoelectron spectroscopy (XPS, Axis Ultra DLD) was carried out using a focused monochromatized Al-Kα radiation (1486.6 eV) to determine the change in the chemical state of various functional groups in GO before and after chemical reduction. The XPS spectra were fitted using the XPSPeak 4.0 software. The structural changes of GO and RGO-CNT after chemical reduction were measured with an X-ray diffractometer with Cu Kα radiation ($\lambda = 0.15418$ nm) under a voltage of 40 kV and a current of 30 mA.

BET measurement. Specific surface area analysis was carried with Quantachrome Instruments and with the Brunauer-Emmett-Teller (BET) method using nitrogen adsorption.

Electrical conductivity measurements. The volume conductivity of PS composite films higher than 10^{-6} S/m was measured by a four-probe method using RTS-9 resistivity measurement system. For samples with a volume electrical conductivity below 10^{-6} S/m, they were studied using a PC-68 high-resistance meter (Shanghai Jingmi Instrument Co., China). There were not any treatments on the sample surface to adjust the contact resistance between samples and measuring electrodes. The conductivity results reported are the mean value of five replicate measurements

8

3. Results and discussion

3.1 Design strategy of constructing 3D hierarchical structure of RGO-CNTin CPC.

The essence of our design strategy to construct a proper 3D hierarchical multi-scale structure of RGO-CNT in CPC is schematically depicted in Figure 2. The sketch of the final composite illustrates that the key design concept is to construct 3D foam-like conducting network structure of RGO-CNT in a PS matrix. The design comprises the following design elements: (a) amphiphilic GO is employed to disperse pristine CNTs to yield a homogeneous aqueous dispersion through π- π interaction. (b) water-soluble PVP grafted on PS microsphere surface allows GO-stabilized CNTs to self-assemble on the PS microsphere surface during latex blending through hydrogen bonding between GO and PS microsphere surface (see Figure 1S); PS microspheres can act as template for the formation of ordered 3D foam-like conductive network by directing the conductive nano-fillers to distribute along boundaries of PS microspheres; (c) the resultant GO-CNT-PS microsphere is *in-situ* reduced by an HI solution. In this process, GO is reduced back to conductive reduced-GO (RGO) and electrically connects with CNTs; meanwhile, CNTs on RGO can serve as effective spacers to prevent RGO from re-stacking; PS microsphere also immobilizes GO-stabilized CNTs to avoid the irreversible aggregation of RGO-CNTs after chemical reduction; (d) the resultant RGO-CNT/PS microspheres are hot-pressed to form a composite. This yields a compact 3D conductive structure. During the thermal-press step, 2D RGO sheets wrap each PS microsphere and act as "nano-wall" to prevent CNTs from diffusing into the PS microsphere, which results in a more intact segregated network. Here, the π- π interaction between RGO and CNTs also stabilizes and reinforces the 1D-2D "partnership" for synergetic effect. The RGO-CNT combination has a mechanical strength superior to those of CNT-network or RGO-network.
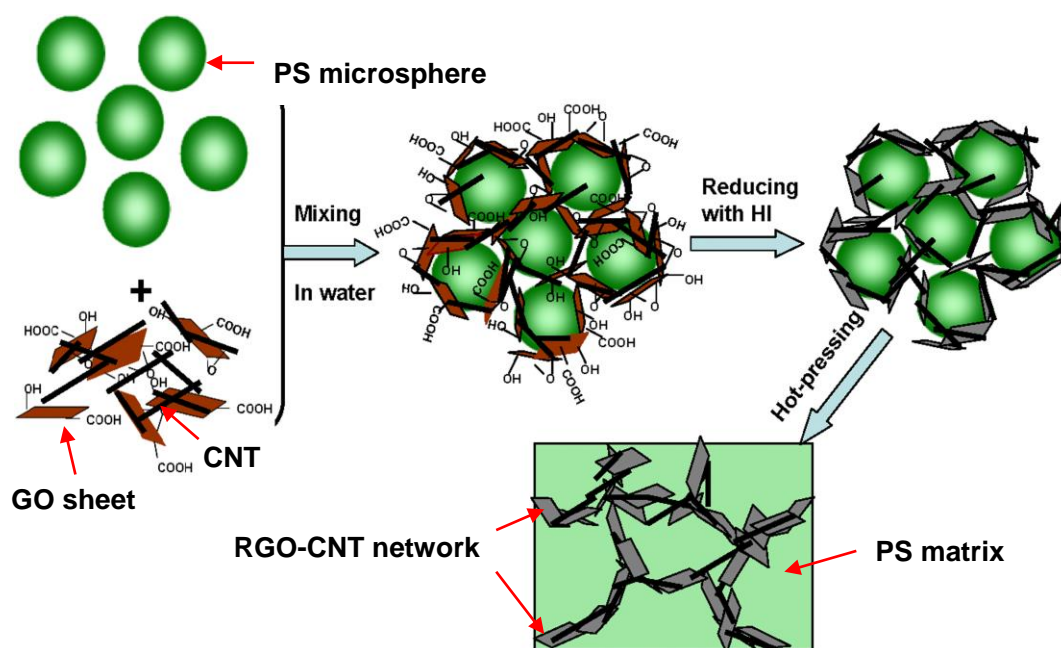
Figure 2. Schematic illustration of preparation of CPC with a 3D foam-like conducting network of RGO-CNT: amphiphilic GO is employed to disperse pristine CNTs to yield a homogeneous aqueous dispersion through π- π interaction; GO-stabilized CNTs self-assemble on PS microspheres by hydrogen bonding interaction and then chemically reduced with HI solution to form RGO-CNT/PS microsphere powder. Finally, the resultant powder is hot-pressed to form the CPC with desirable structure.

3.2 Dispersing pristine CNTs by using GO.

Figure 3a and b show the statistical histograms of lateral size and thickness for GO sheets (measured from AFM images in Figure 2S). Most GO are irregularly shaped sheets with size ranging from 500 nm to 4.5 μm. The average thickness of GO sheets is close to 0.9 nm, indicating that our raw graphite was successfully exfoliated into single-layer or few-layer-stacked GO sheets. As-prepared GO sheets have a lot of highly hydrophilic groups (e.g. hydroxyl, epoxy, and carboxyl groups) [36] and readily dissolve in water to form a brownish solution (Figure 3c). However, pristine CNTs are hydrophobic and tend to aggregate in water due to their poor wetting with water. The addition of surfactant (e.g. SDS) makes CNTs soluble in water by their hydrophobic

10
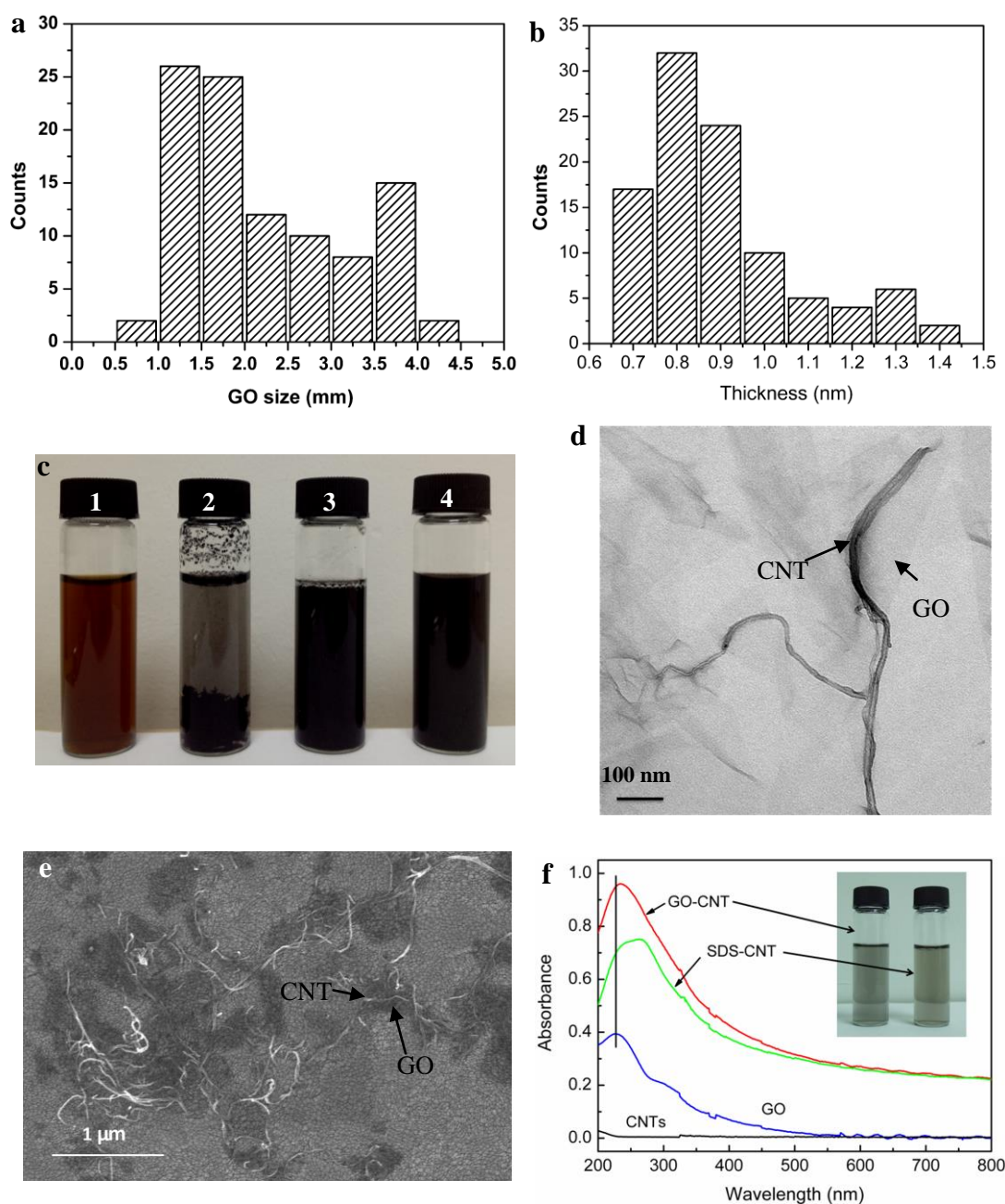
Figure 3. Histograms showing the variation of the lateral size (a) and the thickness (b) for GO sheets, respectively; (c) photos of the vials containing the aqueous dispersions of GO (1), pristine CNT (2), SDS-CNT (3), and GO-CNT (4) after sonication treatment, respectively; TEM image (d) and SEM image (e) of GO-CNT dispersion after drying; (f) UV-Vis absorption spectra of aqueous dispersions of pristine CNT, GO, SDS-CNT and GO-CNT. The concentrations of two CNT suspensions are both 0.0125 mg/ml, and the weight ratios of SDS and GO to CNTs are kept at 1:1.

11

interaction [42]. GO is found to be an effective surfactant that can stabilize CNTs in water to yield a homogenous black solution (Figure 3c). The effectiveness in dispersion is attributed to the attachment of CNTs on amphiphilic GO sheets (as shown in TEM image of Figure 3d) as well as the electrostatic repulsion arising from partially charged GO sheets [40]. SEM image (Figure 3e) also shows that most CNTs can absorb on GO sheets and form good dispersion.

In this work, we used UV-Vis measurements (Figure 3f) to evaluate the aqueous dispersion of pristine CNTs by GO and by SDS. For a solution with dispersed GO or CNTs, the sp^2 carbon materials should show UV absorption. No obvious absorption peak in pristine CNT solution was observed, because CNTs are poorly dispersed in water and they usually precipitate out. With the addition of GO or SDS, the absorbance of CNT aqueous solutions increases, indicating the enhanced dispersion of CNT suspension by either SDS or GO. Considering that both GO and SDS have no absorbance at wavelength below 500 nm, the absorbance within 500-800 nm region can be used to examine the quality of CNT dispersion [43]. It is found that the absorbance in the range of 500-800 nm of GO-stabilized CNT dispersion is close to that of SDS-stabilized CNT dispersion, suggesting that GO has similar dispersing ability for CNTs as SDS. The absorption peak of GO at 227 nm assigned to the $\pi \rightarrow \pi^*$ transition of aromatic C-C bonds red-shifted to 236 nm when GO is mixed with CNTs, which gives a strong proof to the presence of strong π-π stacking interaction between GO sheets and CNTs [44].
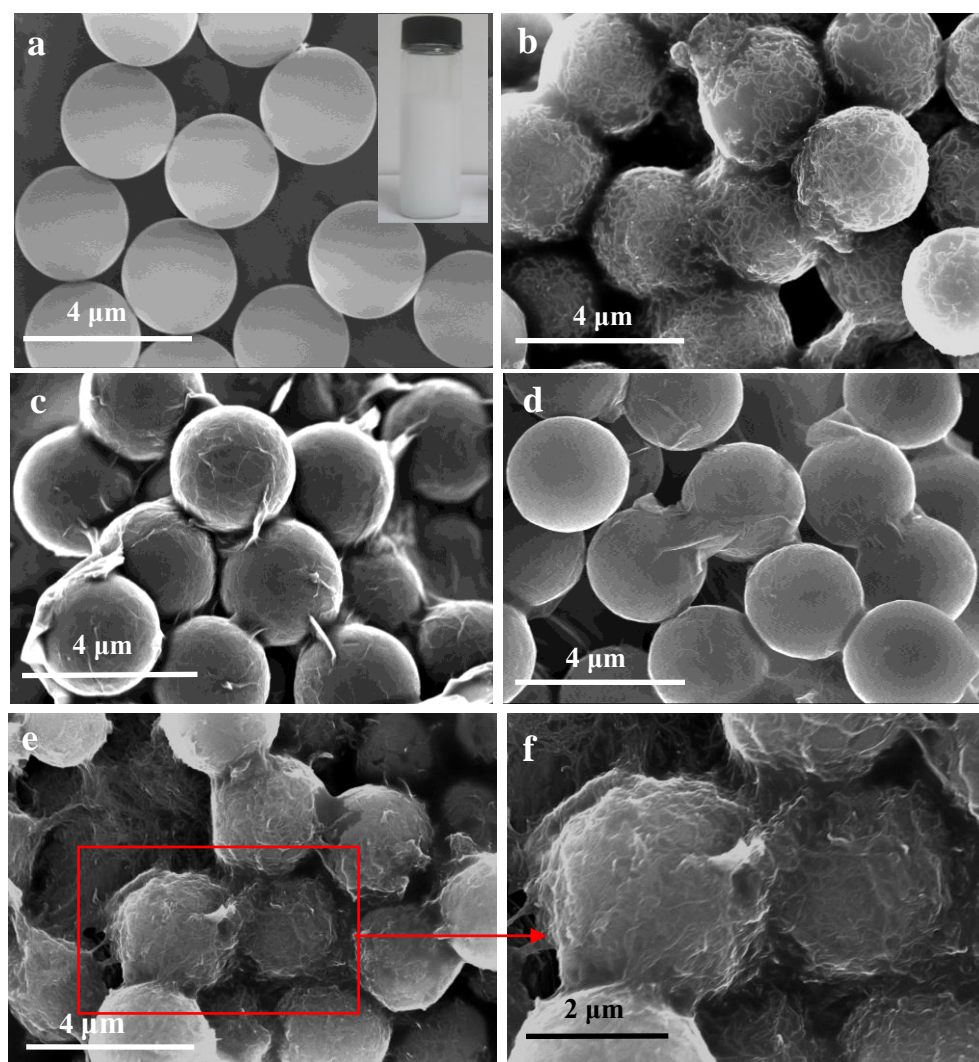
Figure 4. SEM images of (a) PS, (b) SDS-CNT/PS, (c) GO/PS, (d) RGO/PS, and (e) RGO-CNT/PS microspheres, respectively. (f) is the magnified image of (e). The inset in (a) shows the white aqueous dispersion of PS microspheres.

3.3 Formation of hybridized RGO-CNT on PS microspheres via self-assembly and chemical reduction.

Figure 4a shows the SEM image of mono-dispersed PS microspheres with a diameter of ~3 μm prepared by dispersion polymerization. These microspheres easily form a well-dispersed white colloid solution in water due to the water-soluble PVP grafted on their surfaces [36]. Due to rich polar functionalities from SDS or GO, SDS- or GO–stabilized CNTs (as indicated by FTIR in Figure 3S) can mix well and

13

self-assemble on PS microspheres in water. SEM images (Figure 4) confirm that GO-CNTs, SDS-CNTs and GO all coat the PS microspheres effectively and they connect neighboring microspheres after latex mixing.   The self-assembly is driven by various physical interactions between GO sheets and PS microspheres including hydrogen-bonding and π-π stacking.

Owing to the nature of 2D soft material and large aspect ratio of GO sheets, GO sheets not only can carry CNTs to adsorb and conform on the PS latex microspheres but also can connect adjacent PS latex microspheres like glue. This facilitates the formation of interconnected 3D conductive filler network. However, GO sheets tend to stack together onto latex microspheres and such aggregation is not desirable. Particularly, RGO sheets densely re-stack after chemical reduction (as shown in Figure 4d)   through inter-layer π-π interaction due to the loss of oxygenated functional groups of GO interlayer [15]. This leads to a significant waste of nano-filler and compromises some unique properties of graphene. We found in this work that the loading of GO with CNTs, re-stacking of GO and RGO can be greatly minimized. Evidently from Figure 4 e and f, the resultant CNTs/ RGO wrapping on PS latexes after reduction of CNTs/GO look loose and messy and CNTs below RGO sheets can still be seen through transparent RGO sheets. This suggests that CNTs act as spacers to prevent RGO sheets from serious restacking during chemical reduction.
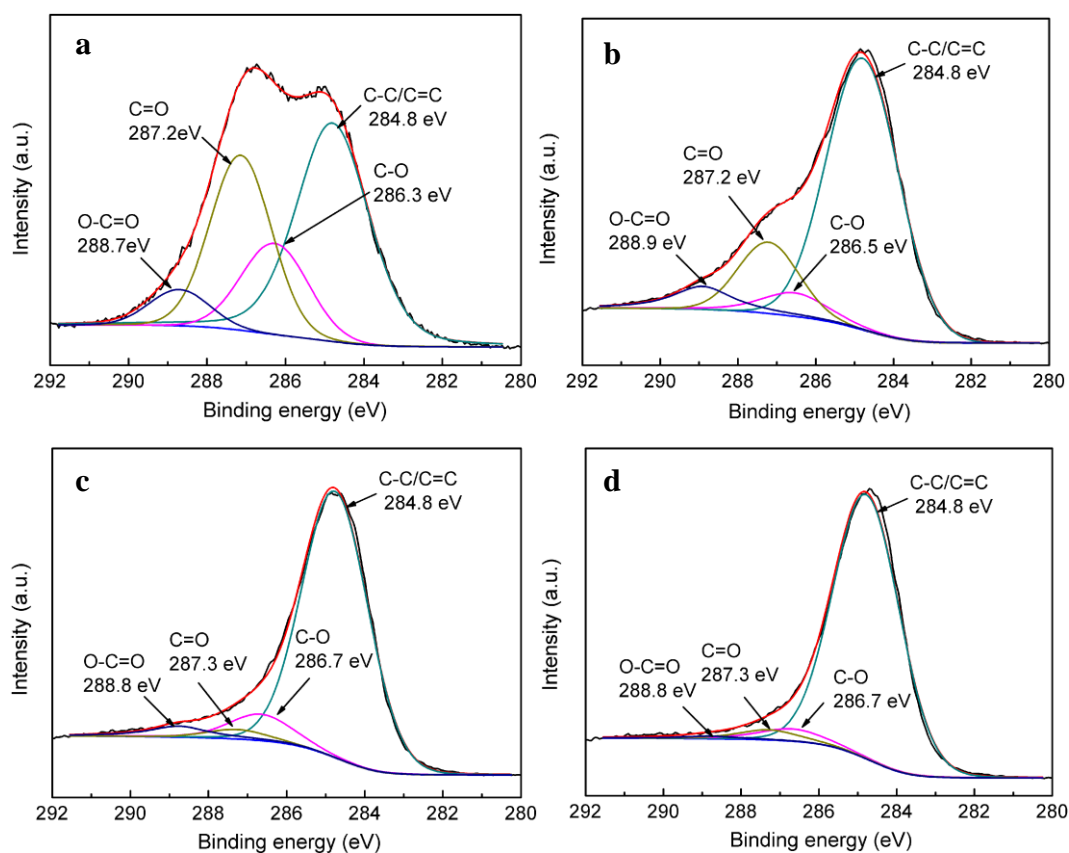
Figure 5. C1s XPS spectra of (a) GO, (b) GO-CNT, (c) RGO, and (d) RGO-CNT.

To evaluate the reduction degree of GO and GO-CNTs on PS microspheres after chemical reduction, we conducted XPS analysis. The resultant RGO and RGO-CNT were extracted by removing PS microspheres in THF solvent prior to XPS analyses. Figure 5 shows the C 1s XPS spectra from GO and GO-CNTs before and after the chemical reduction. Three fitted peaks arising from carboxylic (at 288.7 eV), carbonyl (287.2 eV), and epoxy (286.3 eV) functionalities are clearly identified on GO and GO-CNTs. After chemical reduction with HI, they are all greatly reduced (as shown in Figure 5c and d). The results show that most of the oxygen-containing groups were removed by the HI reduction process. The reduction of GO on PS microspheres into RGO also means that the role of GO is transformed effectively from a dispersant (but electrically insulating) to the role of RGO—a conductive nano-filler is accomplished. Although SDS is also effective in dispersing CNTs, SDS remains electrical insulating

in the entire process of CPC fabrication and the presence of electrical insulators amid the conductive percolation network of CNTs inevitably compromises the resultant conductivity.
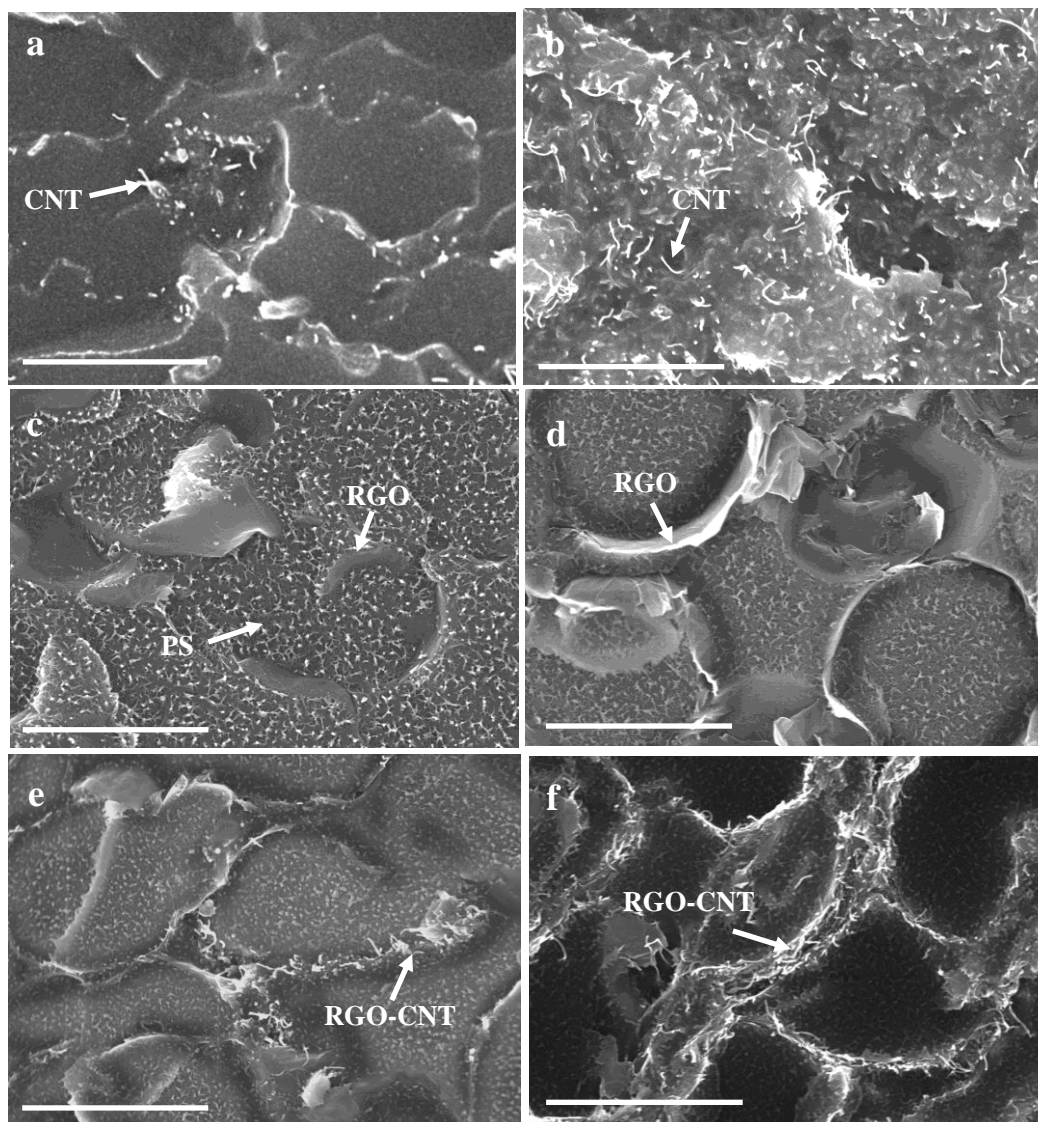
Figure 6. SEM images of cross-sections of PS composites containing (a) 0.5 vol % CNTs, (b) 2 vol% CNTs, (c) 0.5 vol% RGO, (d) 2 vol% RGO, (e) 0.5 vol% RGO-CNTs, (f) 2 vol% RGO-CNTs, respectively. The scale bar is 2 μm.

3.4 3D foam-like conducting network of RGO-CNT in CPC.

In our design strategy, we predict that the final 3D foam-like conducting network structure with a cell size of about 2-3 μm should form and fix after hot-press of PS

microspheres with carbon nano-fillers. Further, all carbon nano-fillers interconnect with each other to form a compact and extended 3D conductive network. The designed carbon nano-filler structures were verified by SEM of the cross-section of a PS composite film after the hot-press step (Figure 6). It is noted that the fiber-like phases appeared in all the composites and PS matrix (Figure 4S) are resulted from the phase separation of PS and PVP. In comparison to CNTs, PVP fibers are very short and dendrite-like, so we can still identify them from their structure characteristics in SEM images. In examining the SDS-CNT/PS composites (Figure 6a), we found that the CNT network structure has a lot of defects where some of SDS-CNTs mixed themselves inside PS microspheres. When the filler concentration was further raised (Figure 6b), we found that more SDS-CNTs entered into PS microspheres from the microsphere boundaries (interfaces) and formed a randomly distributed structure. This phenomenon of losing fillers into the polymer bulk indicates the destruction of segregated CNT network during the thermal-press process in the CPC fabrication. Similar phenomena on filler network structure destruction during polymer deformation and flow were also widely observed in other polymer composite systems, which has been a big barrier to preparation of polymer composites with controllable filler morphology.[27,28,37, 45]. According to the recently proposed "shape-dependent localization of nanofiller in polymer matrix" theory [46], it can be explained that low stability and high transfer speed of low dimensional nano-filler (e.g., 0D carbon-black and 1D CNT) at phase interfaces lead to uncontrolled distribution of SDS-CNT in PS matrix. In addition, our work shows the trend that the uncontrolled and undesirable transfer of CNTs in polymer is stronger with the increase of nano-filler concentration. As such, increasing the amount of conductive nano-fillers is not only ineffective in reinforcing the nano-filler network but even weakens the network and causes filler wastage for constructing conductive pathway.

In contrast, the RGO/PS composite (Figure 6c and d) exhibits a complete 3D segregated network structure even with an increase in filler concentration (*i.e.* graphene). This result suggests that robust graphene with its unique 2D sheet structure closely wrapping the PS microspheres can effectively restrict the flow of the PS melt
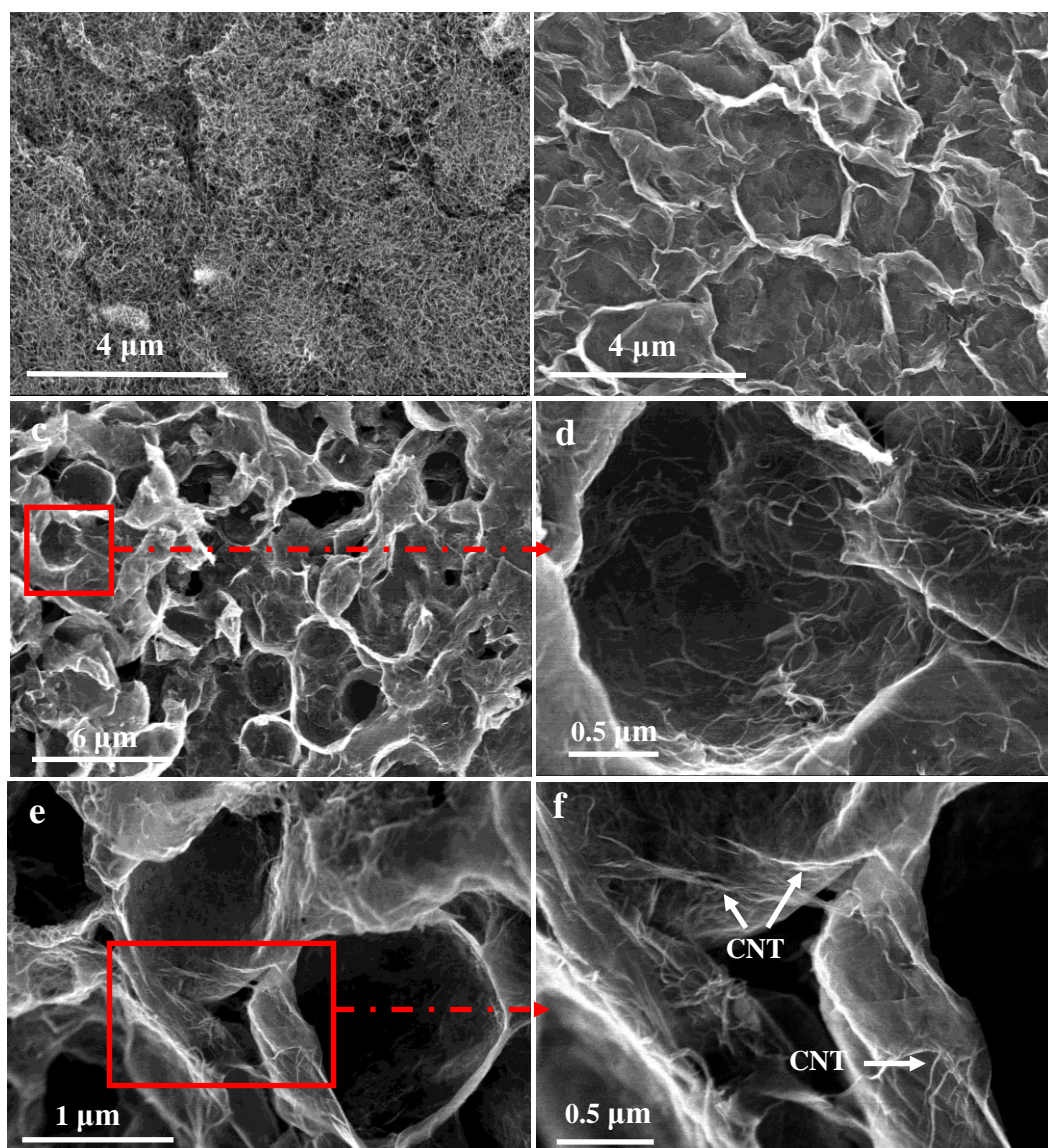
Figure 7. SEM images of extracted nanofiller skeletons from polymer composites by THF: (a) CNT, (b) RGO, (c,d) RGO-CNT at different locations. (e) and (f) are higher magnitude images of (c) and (d), respectively.

and stably pins the filler locations at the microsphere interfaces during hot-pressing. However, we also found that a large number of RGO sheets were confined at the polymer microsphere interfaces. This suggests serious restacking of RGO when the filler concentration is relatively high. Figure 6 e and f show that with the addition of CNTs, the RGO-CNT/PS composites have the strongest filler-stability against the possible damage induced by the hot-pressed step, as well as the least

18

graphene-restacking probability. These characteristics of RGO-CNTs facilitate lowering the percolation and increasing the conductivity for the composite. To the best of our knowledge, our work is the first report that RGO sheets can act as "nano-wall" to restrict the transfer of CNTs at interfaces and a segregated RGO-CNT network with high quality in a polymer matrix can be constructed. This finding means that GO not only can disperse low-dimensional carbon nano-fillers but also can tailor their morphology in CPCs by controlling filler location in the polymer matrix.

To evaluate the quality of 3D RGO-CNT hybrid network and compare its advantage over other single-component filler (RGO or CNT) network, PS composites with various carbon nano-fillers were etched by THF solvent to remove the PS matrix. The residual filler skeletons are shown in Figure 7. It can be seen that the CNT skeleton network (Figure 7a) collapses and forms large aggregates due to the weak connection between 1D CNTs. For the RGO skeleton network (Figure 7b), RGO sheets compactly restack together to form a porous structure. Interestingly, the RGO-CNT skeleton network (Figure 7 c-f) yields a robust 3D foam-like structure with porous cell walls where CNTs penetrate into RGO stacks and interconnect with RGO and CNTs on neighboring foam walls. This implies that combination of RGO and CNTs strengthens the 3D network structure and well keeps the integrity of 3D RGO-CNT hierarchical structure proposed and demonstrated in this work. In addition, the density of RGO-CNT foam skeleton (ρ =0.025 mg/cm^{-3}) is much lower than that of other carbon nanofiller skeletons such as GO, RGO, and CNT (Figure 6S), suggesting the more loose package and larger surface area in RGO-CNT.

XRD and BET measurements were employed to further study the structural characteristics of these 3D conducting filler networks. Figure 8 shows the XRD patterns of GO, RGO, CNTs and RGO-CNTs. GO and CNTs exhibit strong characteristic peaks at 2θ = 11° and 25.7°, respectively. After reduction, the characteristic peak of RGO shifts upward to 2θ = 24.1° due to the decreased interlayer spacing [47], indicating a severe re-stacking of RGO sheets after the surface oxygenated functionalities had been removed by reduction. However for RGO-CNTs, the characteristic peak of stacked RGO is not found and it implies that CNTs remain as
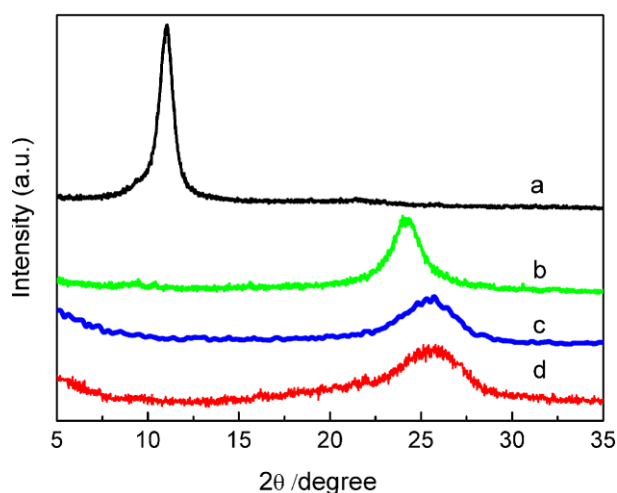
Figure 8.   XRD pattern of (a) GO, (b) RGO, (c) CNT, and (d) RGO-CNT.
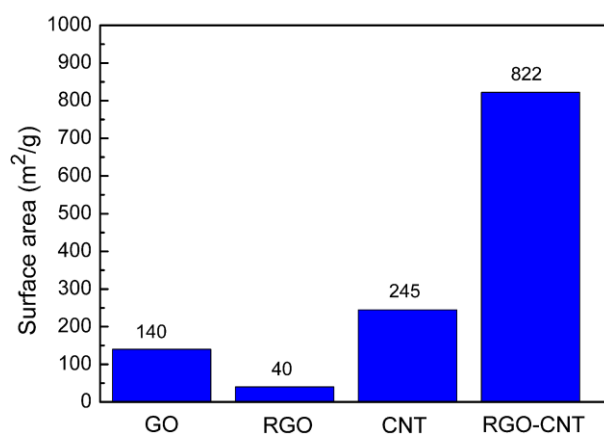
Figure 9. Surface areas measured by BET method for GO, RGO, CNT and RGO-CNT.

spacers in between RGO sheets, and prevent RGO sheets from re-stacking during reduction. The surface areas of GO, RGO, CNTs and RGO-CNT were measured by BET methods (Figure 9). The surface area of GO is reduced by over 3-folds after chemical reduction due to severe RGO stacking after removal of oxygenated functionalities, but the RGO-CNT hybrid exhibits the largest surface area among all tested samples. The result further supports that CNTs prevent the GO and RGO sheets from stacking, leading to a large surface area of RGO-CNT hybrid available for building a highly extensive conductive network. Apparently, GO and CNTs help each

other to achieve finely dispersed and distributed hybrid nano-fillers in a PS matrix.
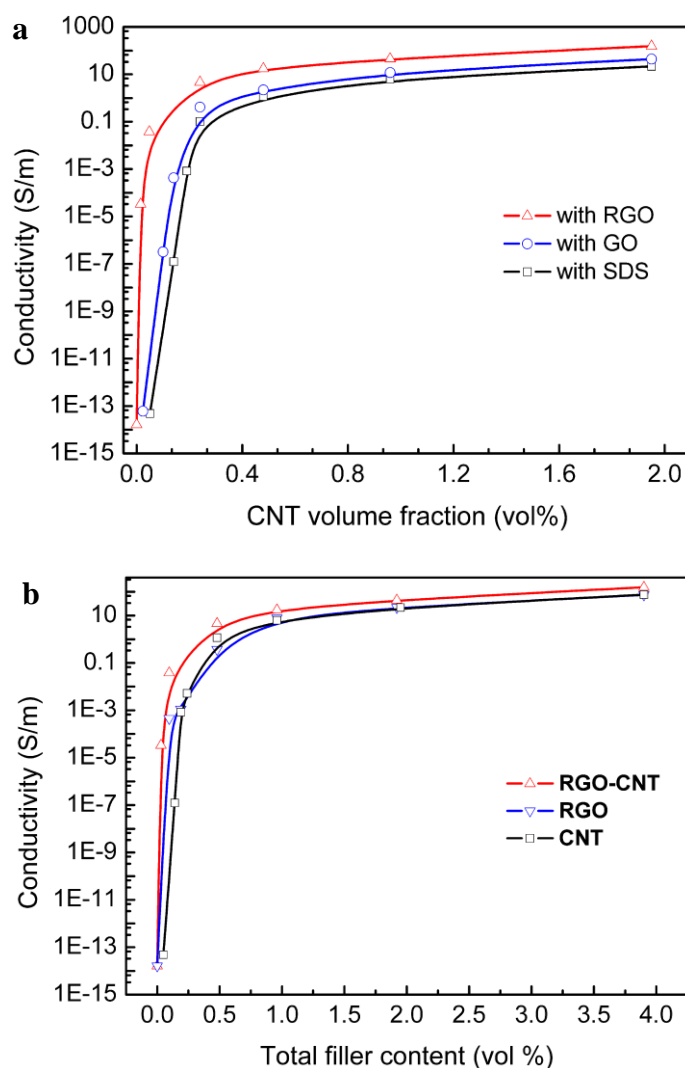
Figure 10. (a) The electrical conductivity of PS composites using GO (RGO) and SDS stabilizers respectively as a function of CNT volume fraction; (b) the electrical conductivity of PS composites as a function of total filler (CNT, RGO, and RGO-CNT, respectively) content.

3.5 Electrical properties of RGO-CNT/PS composites

Figure 10a shows the electrical conductivities of SDS-CNT/PS, GO-CNT/PS and RGO-CNT/PS composites as a function of CNT volume fractions. The plot displays the percolation behavior for the PS composites. Percolation is reached when a sudden

increase in conductivity occurs. The data of electrical conductivity against filler volume fraction is fitted by the classical percolation power law [34]:

$$\sigma = \sigma_0 (\varphi - \varphi_c)^t,$$

where σ is the conductivity of composite, σ_0 is the proportionality constant related to the intrinsic conductivity of filler, φ is the volume fraction of filler, φ_c is the volume fraction of filler at percolation threshold, and t is the critical exponent reflecting the system dimensionality of composites. The SDS-CNT/PS composite shows a percolation threshold of ~0.15 vol% and an ultimate conductivity of 15.5 S/m. The conductivity of GO-CNT/PS composite film is slightly higher than that of SDS-CNT/PS composite film but lower than that of RGO-CNT/PS composite film due to the weak restoration of graphene conductivity by heating during hot-pressing process[36]. With the higher reduction degree of GO by HI, RGO-CNT/PS composite shows an ultralow percolation threshold of 0.015 vol% CNT. Further, the ultimate conductivity of RGO-CNT /PS reaches 153.0 S/m at 2 vol% CNT, which is almost one order of magnitude higher than that of SDS-CNT/PS composite. These results indicate that GO is reduced back to conductive RGO and RGO forms a hybridized conducting network together with CNTs by effective electrical connection. The final conductivity of the SDS-CNT/PS composite is relatively low due to the presence of insulating SDS on CNT as expected.

To further evaluate the synergistic effect in conductivity arising from hierarchical placement of 1D CNTs on 2D RGO in a 3D microsphere template, the conductivity of RGO-CNT/PS composite as a function of total filler volume fractions of CNT and RGO are compared with other CPC containing single filler component (RGO or CNT). The results are summarized in Figure 10b. The RGO-CNT/PS CPC shows an extremely low percolation threshold (0.03 vol% RGO-CNT), which is much lower than those of the RGO/PS (0.1 vol%) and CNT/PS (0.15 vol%) composites. In addition, for the same conductive filler content, the conductivity of the RGO-CNT/PS CPC is also higher than those containing CNT or RGO as the sole filler content. These results confirm the presence of synergetic effect of RGO and CNT, and also

explain the importance of the filler's composition and structure design in lowering the percolation threshold and the ultimate electrical conductivity of the final CPC.

Table 1. **Electrical properties of CPCs using various fillers based on CNT, graphene, and graphene-CNT, respectively.**

Polymer matrix	Filler type	Stabilizer	processing	φ_c for filler (vol%)	σ (S/m)	Ref
PS	MWCNT	SDS	Latex mixing	0.75	1 (2.25 %)	Ref 40
PS	SWCNTs	SDS	Latex mixing	0.2	10 (1 %)	Ref 43
PS	SWCNTs	PEODT :PSS	Latex mixing	0.1	500 (~2%)	Ref 43
PS	Functionalized graphene	Not used	Solvent mixing	0.1	1 (2.5 %)	Ref 46
PS	graphene	PSS	Latex mixing	0.3	15 (2%)	Ref 47
SBS	Graphene-MWCNT	Not used	Solvent mixing	0.125	<1(3%)	Ref 22
PS	Graphene -MWCNT	GO	Latex mixing with Self-assembly	0.03	153 (~4 %)	Our work

PS= polystyrene, PEDOT: PSS= poly(3,4-ethylenedioxythiophene):poly(4-styrenesulfonate) , SBS=poly(styrene-co-butadiene-co-styrene); all percolation thresholds in the composites are reported in volume fraction converted from the weight fraction.

Table 1 compares the electrical properties of our conductive RGO-CNT/PS CPC with the reported CPCs using various filler designs based on CNT, graphene and graphene-CNT[22,40, 48, 49]. For the assurance of relevancy in comparison, reference data are mostly chosen from those using the same PS matrix. Evidently, the electrical properties of our composites with a 3D foam-like RGO-CNT network prepared by our

23

well-designed 3D hierarchical approach are much better than those of composites with graphene, CNT or graphene-CNT as their nano-fillers. Even when our results are compared to a recent work on using SWCNTs and conductive polymer PEODT:PSS as a stabilizer, our RGO-CNT/PS displays a lower percolation threshold. In fact, it is actually the lowest among the available data in the literature to the best of our knowledge. Although the ultimate conductivity achieved with our CNT/RGO/PS approach is lower than that with the PEDOT:PSS-SWCNT approach reported in the literature, PEDOT:PSS is known to be unstable and costly.

(A)

Pure PS   0.15 vol% CNT

0.1 vol% RGO   0.03 vol% RGO-CNT

(B)
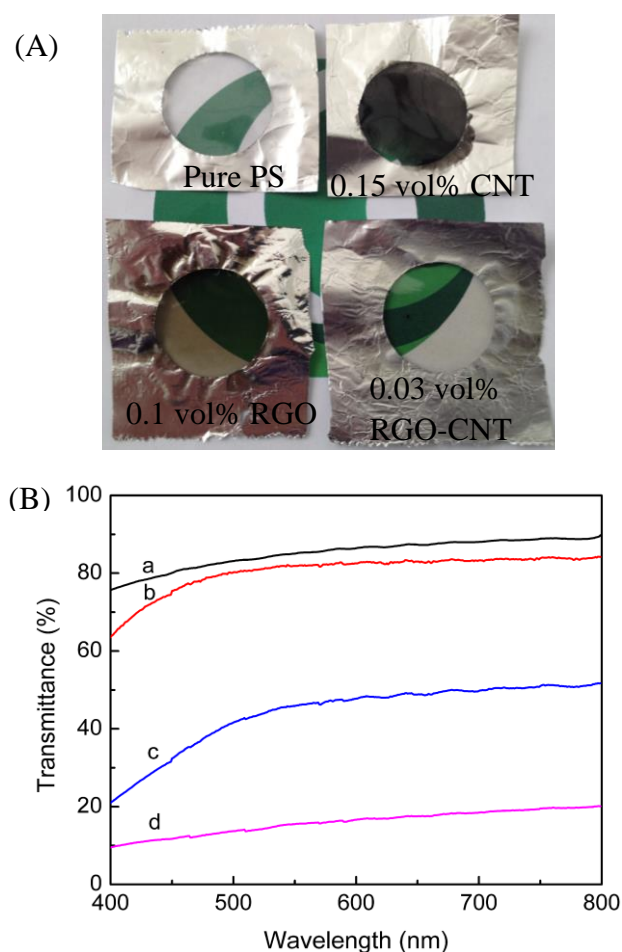
Figure 11. (A) Photographs of (a) pure PS film and PS composite film with various carbon nanofiller contents at percolation threshold. These films with a thickness of ~45μm were formed in the hole of Tin foil by hot-pressing; (B) Optical transmittance spectra of pure PS film and PS composite film shown in including (a) pure PS, (b) 0.03 vol% RGO-CNT/ PS, (c) 0.2 vol% RGO /PS, and (d) 0.3 vol% CNT/PS films.

One of the most important benefits for achieving as low as possible carbon nano-filler percolation threshold is satisfying the emerging applications compromising transparency and electrical conduction characteristics (eg. transparent antistatic coatings, capacitive touch-screen, and transparent electronic devices). The optical properties of pure PS and our CPC films at a low percolation threshold region (0.15 vol% CNT, 0.1 vol% RGO, and 0.03 vol% RGO-CNT) were evaluated by visual observation and optical spectral analyses (as shown in Figure 11). One can see that CPCs derived from a single-filler-component such as CNT/PS and RGO/PS (Figure 11A) were not optically clear and showed a dark tint while composites with a low RGO-CNT content were relatively clear and transparent. The optical spectral analysis (Figure 11B) shows that the transmittance of 0.03 vol% RGO-CNT/PS has a lowest loss of 2-4% in the spectral window of 450-750 nm. The result suggests that the composite with RGO-CNT prepared by our strategy is promising to be optical transparent CPCs with a wide scope of practical applications.

The mechanical properties of the PS composites with SDS-CNT or RGO-CNT were tested (table 1S). With incorporation of SDS-CNT or RGO-CNT into PS matrix, the tensile strength and tensile modulus of the composites can be improved. But the SDS-CNT has the better effectiveness in improving the mechanical properties than RGO-CNT. It is probably attributed to the fact that the homogeneously dispersed CNTs can transfer more stress than the segregated RGO-CNT in the polymer matrix[11]. However, the mechanical properties (tensile strength >15.5 MPa and tensile modulus>2300 MPa) of the composites with RGO-CNT have been able to satisfy their real application.

4.Conclusion

We report a simple, facile, and water-based method to construct a 3D foam-like hierarchical conductive network structure via self-assembly, with conductive carbon nanotubes (CNTs) and graphene sheets as the 1D and 2D nano-constituents and latex-polystyrene microspheres as the 3D micro-building-block. The electrical properties (conductivity of 153 S/m 4 vol% RGO-CNT and percolation threshold of

0.03 vol% RGO-CNT) of CPCs with such 3D hierarchical and multi-scale structures are much better than CPCs with RGO or CNT alone. Particularly, CPCs with the 3D conducting network of RGO-CNT show an extremely low percolation threshold, which is lower than the data current available in the literature on conductive PS composites with carbon nano-fillers. The enhanced properties are attributed to the synergy coming from graphene and CNTs in forming a 3D conducting network with high quality, which is produced by the following key factors: (1) self-assembly method is employed to precisely construct ordered conductive network; (2) π-π interaction between graphene and CNTs also stabilizes and reinforces the 1D-2D "partnership"; (3) GO is used as an alternative stabilizer to insulating surfactants and can be reduced to conductive graphene to electrically connect with CNT; (4) the resultant graphene act as "nano-wall" to prevent CNT from randomly diffusing into the polymer microsphere and effectively keep the integrity of conductive network; (5) CNTs on RGO serve as effective spacers to prevent graphene from re-stacking for producing available large surface area. In addition, achieving a super-low carbon nano-filler percolation threshold by our design strategy would provide a new way for polymer composites with carbon nano-filler to the various applications requiring transparency and conductive characteristics simultaneously.

Nanoscale Accepted Manuscript

Reference

1. A. Cao, P. L. Dickrell, W. G. Sawyer, M. N. Ghasemi-Nejhad and P. M. Ajayan, *Science*, 2005, **310**, 1307-1310.

2. N. Halonen, A. Rautio, A.-R. Leino, T. Kyllönen, G. Tóth, J. Lappalainen, K. Kordás, M. Huuhtanen, R. L. Keiski, A. Sápi, M. Szabó, Á. Kukovecz, Z. Kónya, I. Kiricsi, P. M. Ajayan and R. Vajtai, *ACS Nano*, 2010, **4**, 2003-2008.

3. P. M. Sudeep, T. N. Narayanan, A. Ganesan, M. M. Shaijumon, H. Yang, S. Ozden, P. K. Patra, M. Pasquali, R. Vajtai, S. Ganguli, A. K. Roy, M. R. Anantharaman and P. M. Ajayan, *ACS Nano*, 2013, **7**, 7034-7040.

4. S. Nardecchia, D. Carriazo, M. L. Ferrer, M. C. Gutierrez and F. del Monte, *Chemical Society reviews*, 2013, **42**, 794-830.

5. W. L. Noorduin, A. Grinthal, L. Mahadevan and J. Aizenberg, *Science*, 2013, **340**, 832-837.

6. F. Natalio, T. P. Corrales, M. Panthoefer, D. Schollmeyer, I. Lieberwirth, W. E. G. Mueller, M. Kappl, H.-J. Butt and W. Tremel, *Science*, 2013, **339**, 1298-1302.

7. L. Qiu, J. Z. Liu, S. L. Chang, Y. Wu and D. Li, *Nature communications*, 2012, **3**, 1241.

8. Z. Chen, W. Ren, L. Gao, B. Liu, S. Pei and H.-M. Cheng, *Nature Materials*, 2011, **10**, 424-428.

9. Z.-S. Wu, Y. Sun, Y.-Z. Tan, S. Yang, X. Feng and K. Muellen, *Journal of the American Chemical Society*, 2012, **134**, 19532-19535.

10. P. Huang, W. Chen and L. Yan, *Nanoscale*, 2013, **5**, 6034-6039.

11. C. Tang, L. Xiang, J. Su, K. Wang, C. Yang, Q. Zhang and Q. Fu, *Journal of Physical Chemistry B*, 2008, **112**, 3876-3881.

12. L. Liu and J. C. Grunlan, *Advanced Functional Materials*, 2007, **17**, 2343-2348.

13. W. D. Zhang, I. Y. Phang and T. X. Liu, *Advanced Materials*, 2006, **18**, 73-77.

14. Q. Fu, C. Tang, H. Deng and Q. Zhang, *Polymer Nanotube Nanocomposites: Synthesis, Properties and Applications, ed. by Mittal V. Wiley/Scrivener Publishing, Hoboken, NJ/Salem, MA*, 2010, 83-112.

15. L. Qiu, X. Yang, X. Gou, W. Yang, Z. F. Ma, G. G. Wallace and D. Li, *Chemistry*, 2010, **16**, 10653-10658.

16. H. Y. Mao, Y. H. Lu, J. D. Lin, S. Zhong, A. T. S. Wee and W. Chen, *Progress in Surface Science*, 2013, **88**, 132-159.

17. D. Wei, L. Xie, K. K. Lee, Z. Hu, S. Tan, W. Chen, C. H. Sow, K. Chen, Y. Liu and A. T. S. Wee, *Nature communications*, 2013, **4**, 1374.

18. Z. Yan, L. Ma, Y. Zhu, I. Lahiri, M. G. Hahm, Z. Liu, S. Yang, C. Xiang, W. Lu, Z. Peng, Z. Sun, C. Kittrell, J. Lou, W. Choi, P. M. Ajayan and J. M. Tour, *ACS Nano*, 2012, **7**, 58-64.

19. F. Du, D. Yu, L. Dai, S. Ganguli, V. Varshney and A. K. Roy, *Chemistry of Materials*, 2011, **23**, 4810-4816.

20. P. Chen, T.-Y. Xiao, Y.-H. Qian, S.-S. Li and S.-H. Yu, *Advanced Materials*, 2013, **25**, 3192-3196.

21. S.-H. Lee, V. Sridhar, J.-H. Jung, K. Karthikeyan, Y.-S. Lee, R. Mukherjee, N. Koratkar and I.-K. Oh, *ACS Nano*, 2013, **7**, 4242-4251.

22. M. Chen, T. Tao, L. Zhang, W. Gao and C. Li, *Chemical communications*, 2013, **49**, 1612-1614.

23. Y.-T. Liu, M. Dang, X.-M. Xie, Z.-F. Wang and X.-Y. Ye, *J. Mater. Chem.*, 2011, **21**, 18723.

24. P. M. Ajayan and J. M. Tour, *Nature*, 2007, **447**, 1066-1068.

25. A. Hermann, T. Chaudhuri and P. Spagnol, *International Journal of Hydrogen Energy*, 2005, **30**, 1297-1302.

26. H. Kim, A. A. Abdala and C. W. Macosko, *Macromolecules*, 2010, **43**, 6515-6530.

27. K.-Y. Chun, Y. Oh, J. Rho, J.-H. Ahn, Y.-J. Kim, H. R. Choi and S. Baik, *Nat Nano*, 2010, **5**, 853-857.

28. J. C. Grunlan, A. R. Mehrabi, M. V. Bannon and J. L. Bahr, *Advanced Materials*, 2004, **16**, 150-+.

29. H. Deng, L. Lin, M. Ji, S. Zhang, M. Yang and Q. Fu, *Progress in Polymer Science*, DOI: org/10.1016/j.progpolymsci.2013.07.007

30. A. V. Kyrylyuk, M. C. Hermant, T. Schilling, B. Klumperman, C. E. Koning and P. van der Schoot, *Nat Nano*, 2011, **6**, 364-369.

31. M. Moniruzzaman and K. I. Winey, *Macromolecules*, 2006, **39**, 5194-5205.

32. P. Fratzl and R. Weinkamer, *Progress in Materials Science*, 2007, **52**, 1263-1334.

33. A. Hanisch, A. H. Gröschel, M. Förtsch, M. Drechsler, H. Jinnai, T. M. Ruhland, F. H. Schacher and A. H. E. Müller, *ACS Nano*, 2013, **7**, 4030-4041.

34. Y. Kim, J. Zhu, B. Yeom, M. Di Prima, X. Su, J.-G. Kim, S. J. Yoo, C. Uher and N. A. Kotov, *Nature*, 2013, **500**, 59-63.

35. C. Wu, X. Huang, G. Wang, L. Lv, G. Chen, G. Li and P. Jiang, *Advanced Functional Materials*, 2013, **23**, 506-513.

36. G. Long, C. Tang, K.-w. Wong, C. Man, M. Fan, W.-m. Lau, T. Xu and B. Wang, *Green Chemistry*, 2013, **15**, 821.

37. I. Jurewicz, P. Worajittiphon, A. A. King, P. J. Sellin, J. L. Keddie and A. B. Dalton, *The journal of physical chemistry. B*, 2011, **115**, 6395-6400.

38. C. Tang, T. Zhou, J. Yang, Q. Zhang, F. Chen, Q. Fu and L. Yang, *Colloids and Surfaces B: Biointerfaces*, 2011, **86**, 189-197.

39. K. Balasubramanian and M. Burghard, *Small*, 2005, **1**, 180-192.

40. J. Kim, L. J. Cote, F. Kim, W. Yuan, K. R. Shull and J. Huang, *Journal of the American Chemical Society*, 2010, **132**, 8180-8186.

41. W. S. Hummers and R. E. Offeman, *Journal of the American Chemical Society*, 1958, **80**, 1339-1339.

42. J. Yu, K. Lu, E. Sourty, N. Grossiord, C. E. Koning and J. Loos, *Carbon*, 2007, **45**, 2897-2903.

43. L. Tian, M. J. Meziani, F. Lu, C. Y. Kong, L. Cao, T. J. Thorne and Y. P. Sun, *ACS Appl Mater Interfaces*, 2010, **2**, 3217-3222.

44. C. Zhang, L. Ren, X. Wang and T. Liu, *The Journal of Physical Chemistry C*, 2010, **114**, 11435-11440.

45. M. C. Hermant, B. Klumperman, A. V. Kyrylyuk, P. van der Schoot and C. E. Koning, *Soft Matter*, 2009, **5**, 878-885.

46. A. Göldel, A. Marmur, G. R. Kasaliwal, P. Pötschke and G. Heinrich, *Macromolecules*, 2011, **44**, 6094-6102.

47. S. Pei, J. Zhao, J. Du, W. Ren and H.-M. Cheng, *Carbon*, 2010, **48**, 4466-4474.

48. S. Stankovich, D. A. Dikin, G. H. B. Dommett, K. M. Kohlhaas, E. J. Zimney, E. A. Stach, R. D. Piner, S. T. Nguyen and R. S. Ruoff, *Nature*, 2006, **442**, 282-286.

49. E. Tkalya, M. Ghislandi, A. Alekseev, C. Koning and J. Loos, *Journal of Materials Chemistry*, 2010, **20**, 3035-3039.